scientific reports

Check for updates

OPEN

V_m-related extracellular potentials observed in red blood cells

Michael Pycraft Hughes[1]✉, Emily J. Kruchek[1], Andrew D. Beale[1,4], Stephen J. Kitcatt[1], Sara Qureshi[1], Zachary P. Trott[1], Oriane Charbonnel[1,2], Paul A. Agbaje[1], Erin A. Henslee[1,5], Robert A. Dorey[1], Rebecca Lewis[3] & Fatima H. Labeed[1]

Even in nonexcitable cells, the membrane potential V_m is fundamental to cell function, with roles from ion channel regulation, development, to cancer metastasis. V_m arises from transmembrane ion concentration gradients; standard models assume homogeneous extracellular and intracellular ion concentrations, and that V_m only exists across the cell membrane and has no significance beyond it. Using red blood cells, we show that this is incorrect, or at least incomplete; V_m is detectable beyond the cell surface, and modulating V_m produces quantifiable and consistent changes in extracellular potential. Evidence strongly suggests this is due to capacitive coupling between V_m and the electrical double layer, rather than molecular transporters. We show that modulating V_m changes the extracellular ion composition, mimicking the behaviour if voltage-gated ion channels in non-excitable channels. We also observed V_m-synchronised circadian rhythms in extracellular potential, with significant implications for cell–cell interactions and cardiovascular disease.

Since the work of Galvani[1], it has been known that electricity plays a role in biological function. Subsequent work by Nernst[2], Goldman[3] and Hodgkin and Katz[4] showed that the ionic imbalance between intracellular and extracellular spaces creates an electrochemical potential (termed the membrane potential V_m) which plays a fundamental role in the function of muscle and nerves[5]. The standard expression for membrane potential is given by the Goldman-Hodgkin-Katz (GHK) equation, thus[3]:

$$V_m = \frac{RT}{F} ln\left(\frac{P_{Na^+}\left[Na^+\right]_{out} + P_{K^+}\left[K^+\right]_{out} + P_{Ca^{2+}}\left[Ca^{2+}\right]_{out} + P_{Cl^-}\left[Cl^-\right]_{in}}{P_{Na^+}\left[Na^+\right]_{in} + P_{K^+}\left[K^+\right]_{in} + P_{Ca^{2+}}\left[Ca^{2+}\right]_{in} + P_{Cl^-}\left[Cl^-\right]_{out}}\right) \quad (1)$$

where $[X]_{out}$ and $[X]_{in}$ are the extracellular and intracellular concentrations of the relevant ions, P_X are the permeability coefficients of the relevant ions, R and F the gas and Faraday constants, and T is the temperature. In non-excitable cells, V_m remains relatively constant (or "resting"), but the resting value varies considerably from one cell type to another[6]. Many mammalian cells exhibit a V_m about − 70 mV with respect to their surroundings, whilst red blood cells (RBCs) are nearer to − 10 mV. Voltages are maintained through membrane-based ion channels that regulate intracellular ion concentrations and transmembrane ion flows[7]. These in turn can be measured as resistances of the membrane and cytoplasm; changes in such properties have been shown to manifest during many cellular phenomena, including cancer metastasis[8] and stem cell differentiation[9]. Recent work in our lab has shown that RBCs exhibit circadian rhythm variations in both membrane resistance and V_m, driven by changing levels of cytoplasmic K^+ and suggesting V_m may play a role in cellular clocks[10,11].

However, V_m is not the only electrical phenomenon which cells exhibit. The cell's (typically negative) surface charge attract counterions, and repel coions or other negatively charged bodies in a region known as the electrical double layer, whose thickness is defined by the Debye screening length

$$1/\kappa = \sqrt{\left(\frac{\varepsilon RT}{2czF^2}\right)} \quad (2)$$

where z is the counterion valency and c the electrolyte concentration (mol m^{-3}). The distribution of ions in the double layer is determined by the balance between electrostatic forces and thermal agitation, obtained by

[1]Centre for Biomedical Engineering, University of Surrey, Guildford, Surrey GU2 7XH, UK. [2]School of Engineering, École Centrale de Lyon, 36 Avenue Guy de Collongue, 69134 Écully, France. [3]School of Veterinary Medicine, University of Surrey, Guildford, Surrey GU2 7XH, UK. [4]Present address: MRC Laboratory for Molecular Biology, Francis Crick Avenue, Cambridge CB2 0QH, UK. [5]Present address: Department of Engineering, Wake Forest University, 55 Vine St, Wake Downtown, Winston-Salem, NC 27109, USA. ✉email: m.hughes@surrey.ac.uk

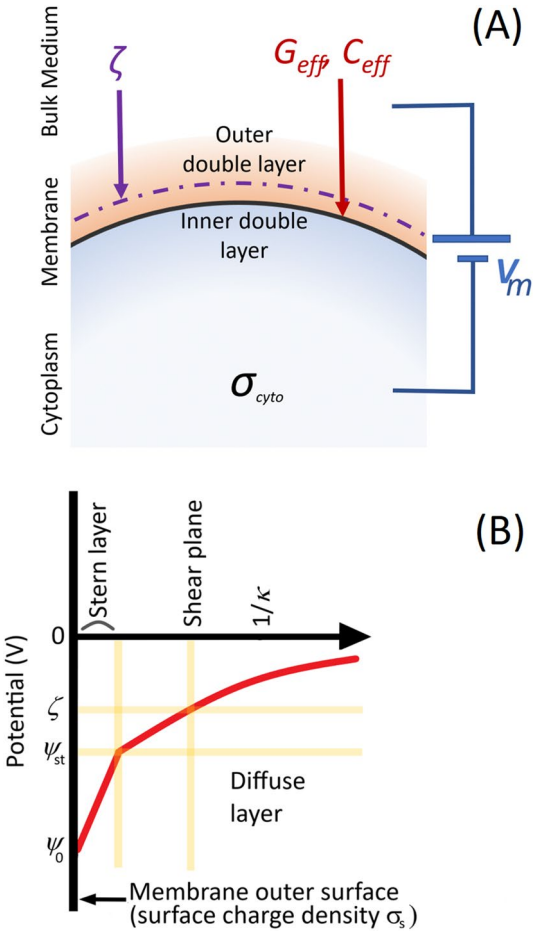

Figure 1. (**A**) A schematic of the cell, indicating the location of the electrical double layers, the shear plane (broken purple line) of ζ, the specific membrane conductance G_{eff} and capacitance C_{eff}, cytoplasm conductivity σ_{cyto} and membrane potential V_m. (**B**) The variation in potential from the cell surface, showing the location of the Stern layer and the shear plane at which ζ is located.

combining the Poisson equation with the Boltzmann distribution, leading to the Gouy-Chapman model[12] which considers the electrical potential $\psi(r)$ as a function of distance from the surface charge into an electrolyte, taking into account screening by counterions. Stern[13] advanced model by adding a surface layer where the number density of ions 'bound' to the charged surface is unaffected by the ionic concentration of the electrolyte, whilst other ions the form a diffuse layer around the particle. The electrostatic potential falls exponentially from the potential at the end of the Stern layer ψ_{St}; the electrical potential at distance r from the surface is given by

$$\psi(r) = \psi_{St} e^{-(\kappa r)}, \tag{3}$$

as shown in Fig. 1. The presence of the countercharge in the double layer immediately outside the cell membrane makes direct measurement of the surface charge difficult; however, its influence can be measured in the electrical potential $\psi(r)$ at the hydrodynamic plane of shear (ca. 1 nm outside the membrane), which marks the plane inside which the ions which act as if attached to the particle. The voltage at the shear plane is called the ζ-potential[12,14]. In theory, ζ is a product of cellular surface chemistry (principally sialic acid residues) and double layer thickness. ζ-potentials have been studied in a number of cells, particularly in RBCs where changes in ζ have been associated with the formation of rouleaux and changes in the erythrocyte sedimentation rate ESR[15,16]. It is also known that RBCs stored for long periods are known to exhibit a reduction in ζ over time[17].

Since V_m is dependent on ion transport through the membrane, there is a strong case that the electrical double layer plays a role in determining V_m. As is clear from the Gouy-Chapman model, the ion concentration at the cell surface is equal not the concentration in the bulk, as used in the GHK equation. Instead, the ion concentration at the surface is described by the Poisson–Boltzmann equation[12]:

$$c_i(0) = c_{oi} exp\left(\frac{-z_i e \Psi}{kT}\right) \tag{4}$$

where $c_i(0)$ is the concentration of ion i at the Stern layer, c_{oi} is the concentration of the ion in the bulk, z is the valency, and e is the charge. Ions carrying the same charge as the cell surface (coions) are electrostatically repelled

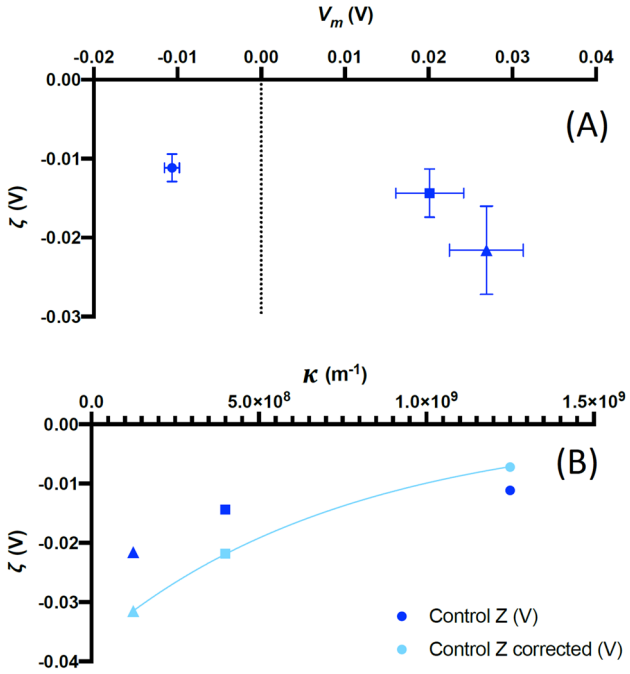

Figure 2. (**A**) The mean variation (± s.d.) in V_m and ζ for control RBCs in media containing 100% (square), 10% (circle) and 1% (triangle) physiological saline as described in the text. (**B**) The same values of ζ plotted against the calculated reciprocal Debye length κ for each medium, together with values adjusted by 0.37 V_m. The relationship between these variables theoretically follows a negative exponential to which the adjusted values offer a perfect ($r^2 = 1$) fit. All points represent the average of four donors.

by charges of like sign, resulting in diminishing coion concentration near the surface; conversely, the counterions increase in concentration near the surface by electrostatic attraction. Such factors are typically considered to be part of the permeability coefficients of the GHK equation. However, the reverse is not taken to be true; the membrane potential affects does not affect the extracellular ion concentration. The effect is taken to be causal in entirely one direction.

We examined V_m and ζ of red blood cells (RBCs) subject to fifteen combinations of ionic strength and surface treatments intended to modify either V_m or ζ, and observed transient changes in both parameters on both short (minute) and long (daily) timescales. We report that whilst V_m is affected by ζ, V_m also alters ζ by up to 37% of V_m via capacitive coupling between the cell interior and the bulk medium. Furthermore, the best-fit model to behaviour also accurately describes observed behaviour attributed to RBCs, including mimicking the behaviour of voltage-activated ion channels in patch-clamp experiments, for which no such channels have been identified.

Results

ζ exhibits V_m-dependence in RBCs. We first considered untreated RBCs, which we examined in three isosmotic media with different ionic strengths (referred to here as 100%, 10% and 1% according to the proportion of saline in the medium, with the remainder comprising iso-osmotic sugar solution (see Methods for details). Lowering ionic strength is known to change V_m in RBCs[18,19], but also changes the thickness of the double layer which is dependent on ionic concentration (see Eq. (2)). Cells equilibrated for 30 min before measurements commenced; the relationship between V_m and ζ is shown in Fig. 2a. Equation (3) suggests that ζ should depend on $1/\kappa$ with ψ_{St} constant. However, when we plotted measured values of ζ against calculated values of κ from Eq. (2) and attempted to fit Eq. (3) to these points, we found the fit was greatly improved through the addition of a term proportional to V_m (as shown in Fig. 2b). The best fit was obtained by calculating ζ from Eq. (3) plus an additional term proportional to V_m and independent of double-layer thickness the ion concentration in the medium. When we included a coefficient of proportionality, Ξ, between V_m and the change in ζ, the best fit is achieved when:

$$\begin{aligned} \zeta &= \psi_{St} e^{-(\kappa x)} + \Xi V_m \\ &= \zeta' + \Xi V_m \end{aligned} \tag{5}$$

where ζ' is the component of the ζ-potential due *only* to the surface charge. When ΞV_m was included, the fit for ζ and κ improved significantly, with a perfect fit ($r^2 = 1$) between Eq. (4) and the data achieved when $\Xi = 0.37$, $\psi_{St} = -0.037$ mV, and the shear plane is 1.0 nm from the end of the Stern layer.

We extended this observation by observing dynamic changes in both V_m and ζ. It is known[18,19] that the V_m of RBCs changes rapidly immediately after resuspension in low ionic strength solution, before reaching steady state some 30 min later. We investigated whether this could be observed in both V_m and ζ by measuring at ≤ 5 min

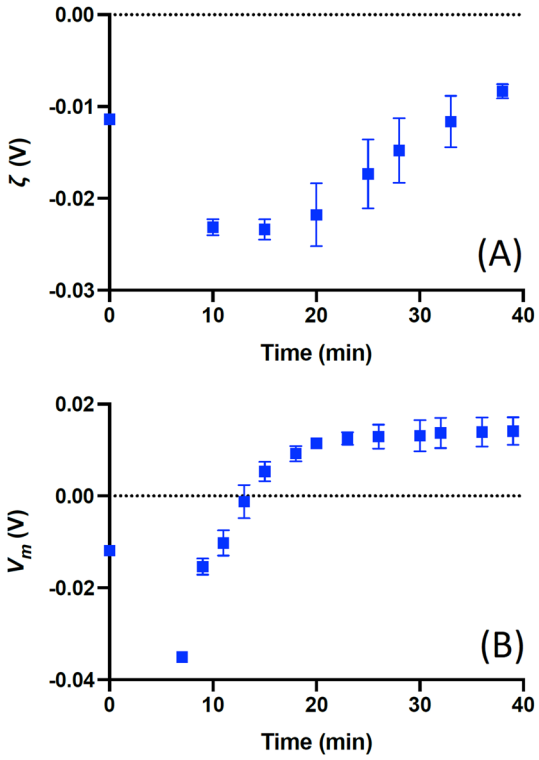

Figure 3. The mean ($n = 3$) V_m (**A**) and ζ-potential (**B**) of RMCE immediately after resuspension into 10% solution (see text). As can be seen, in both instances the value immediately changes from a rest value (taken in 100% solution, denoted here as time 0), peaks and then increases to a rest value. The transition period was consistent for both V_m and ζ, but the former was observed to respond consistently across all three samples, whereas for ζ a delay of 5–15 min was observed before transition began.

intervals after resuspension in 10% medium. The results (Fig. 3) show similar peaks in both V_m and ζ immediately after resuspension, which then transited to a new steady-state value over approximately 20 min. Interestingly, whilst changes in V_m showed little variation in timing across the samples, measurements of ζ exhibited a pause of between 5–15 min before beginning equilibration. However, once the equilibration in ζ began, it took place at the same rate as measurements in V_m; once this delay was taken into consideration, comparison of measured values of V_m and ζ suggests $\Xi = 0.35$ across all samples.

Alteration of the membrane alters the relationship between ζ and V_m. We then repeated the experiment with cells treated using chemical agents to alter the membrane properties. Cells were treated with valinomycin (previously demonstrated to hyperpolarize RBCs)[10], neuraminidase (which removes charge groups from sialic acids on the membrane surface)[20] and a combination of both. Finally, a vehicle control (DMSO, used to dissolve valinomycin) was also studied. When cells were suspended in 100% saline solution, we found that neuraminidase lowered ζ with respect to untreated cells, as expected. However, valinomycin (which alters V_m but does not alter the membrane surface charge) altered both V_m and ζ. Combining neuraminidase and valinomycin produced an additive effect of the two treatments administered separately; when cells were suspended in isosmotic media of different ionic strength, a similar trend was observed (Fig. 4) to that seen for untreated RBCs. As before, superior fits were observed using Eq. (5) than Eq. (3). Neuraminidase fitted ($r^2 = 1$) with $\Xi = 0.19$; where DMSO was used (i.e. treatments of valinomycin, valinomycin + neuraminidase, or vehicle control), optimal fits ($r^2 = 1$) were achieved when $\Xi = 0.085 \pm 0.018$. Estimated values of $\psi_{St,}$ the location of the shear plane x and the value of Ξ used can be seen in Table 1.

The relationship between ζ and V_m is unaffected by double layer thickness or medium composition. We repeated this procedure using untreated RBCs suspended in four isosmotic solutions of different ionic composition, changing both V_m and the thickness of the double layer $1/\kappa$. The solutions used were: (i) 145 mM KCl; (ii) 145 mM NaCl; (iii) 72.5 mM KCl and 72.5 mM NaCl; and (iv) 97 mM $CaCl_2$. We compared the value of ζ measured by electrophoretic mobility with V_m calculated using the GHK equation (Eq. (1)) inserted into Eq. (5) to investigate the relationship between ζ and ψ_{St}. We found that the best fit was achieved when $\Xi = 0.27$; assuming $x = 0.7$ nm as before. This yielded estimates of $\psi_{St} = -30.0 \pm 2.5$ mV for all four cases (Table 2), similar to the values determined in the first study. That this holds for all four cases is notable, as whilst (from Eq. (2)) the double layer is substantially thinner for $CaCl_2$ due to the divalent ion Ca^{2+}, Ξ remains the same, suggesting Ξ is independent of double-layer thickness.

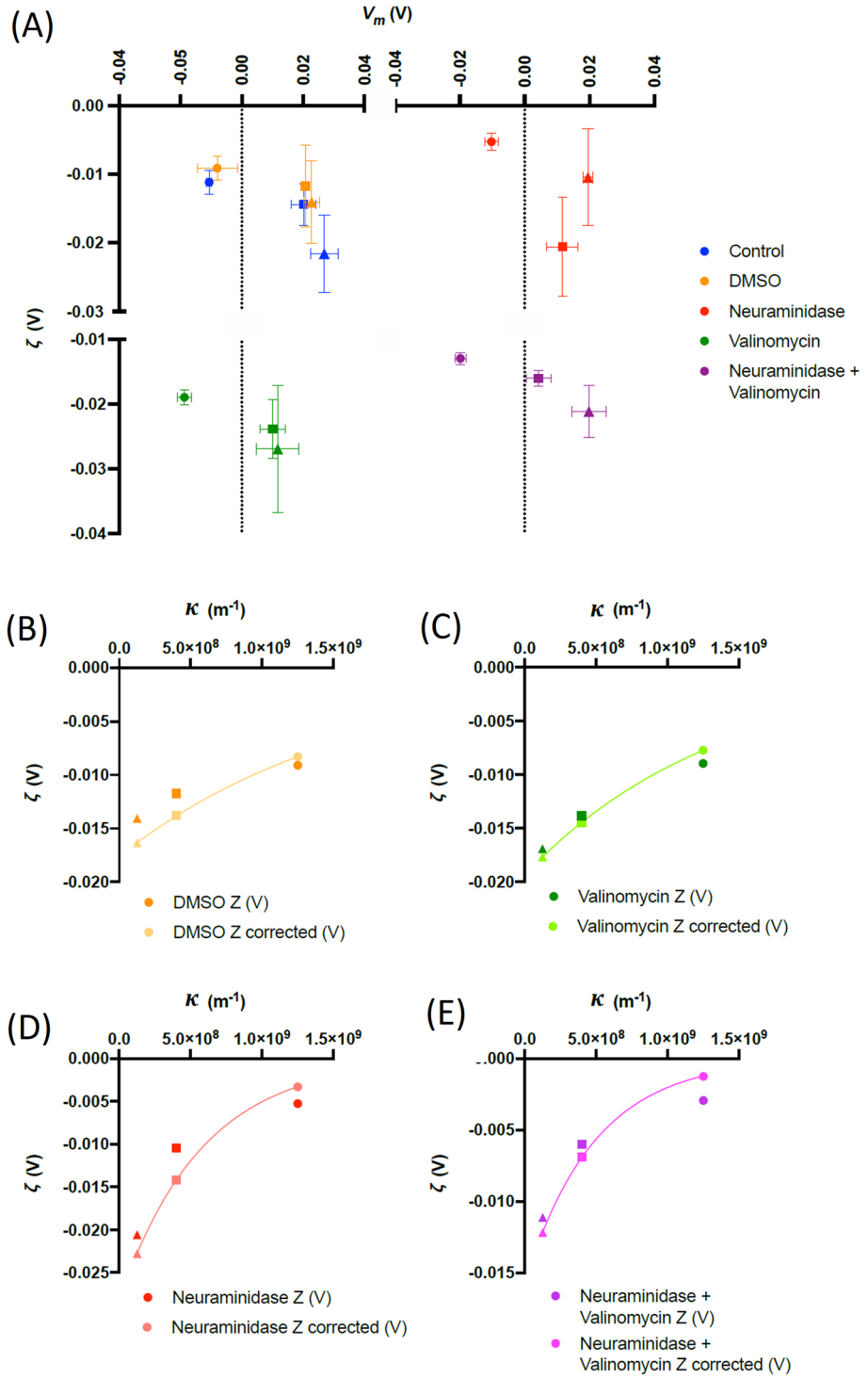

Figure 4. (**A**) The mean variation (± s.d.) in V_m and ζ for RBCs suspended in media containing 100% (square), 10% (circle) and 1% (triangle) physiological saline as described in the text. RBCs were treated with valinomycin, neuraminidase, and a combination of both, as well as a DMSO was control. All points represent the average of four donors. (**B**–**E**) The values of ζ from Fig. 4A plotted against the reciprocal Debye length κ, together with values adjusted by ΞV_m as described in the text. The relationship between these variables theoretically follows a negative exponential, to which the adjusted values offer a perfect ($R^2 = 1$) fit. All points represent the average of four donors.

	Ψ_{St} (V)	X (nm)	Ξ	$C_{shear,}$ Fm^{-2}	Ψ_{St} Ratio	C_{shear} Ratio
Control	− 0.037	1.0	0.37	0.232	1	1
+ Valinomycin	− 0.020	0.7	0.07	0.123	0.54	0.53
+ Neuraminidase	− 0.028	2.0	0.19	0.175	0.76	0.75
+ Valinomycin + Neuraminidase	− 0.016	2.0	0.09	0.100	0.43	0.43
DMSO Control	− 0.018	0.6	0.1	0.125	0.49	0.54

Table 1. Estimated electrical properties for RBCs. The estimated values of surface potential Ψ_{St} and shear plane thickness from the best fit curves shown in Figs. 2 and 5 after adjusting ζ by an amount Ξ multipled by the measured V_m. When the capacitance between shear plane and membrane C_{shear} was calculated, the Ψ_{St} ratios and C_{shear} ratios show a high degree of similarity.

	Measured ζ (V)	Estimated V_m from GHK (V)	V_m (V)	Estimated ψ_{St} (V)
NaCl	− 0.0091 ± 0.0027	− 0.014	0.0058	− 0.034
KCl	− 0.0108 ± 0.0012	− 0.001	0.0008	− 0.028
NaCl/KCl (50:50)	− 0.0090 ± 0.0021	− 0.008	0.0030	− 0.028
CaCl2	− 0.0027 ± 0.0026	− 0.060	0.0088	− 0.030

Table 2. Estimated electrical properties of RBCs in different ionic media. The measured value of ζ in different ionic media, together with the calculated value of V_m for each medium determined using the GHK equation. We used the calculated value of V_m to determine a $\Xi = 0.27$, and determine ζ' using Eq. (5). This was used in Eq. (4) to estimate ψ_{St} due solely to the surface charge, which showed a high degree of similarity across the four cases.

V_m-dependence also affects the passive electrical properties. We also examined the passive electrical properties of effective membrane conductance G_{eff} and capacitance $C_{eff,}$ and cytoplasm conductivity σ_{cyto} of the cells in 100%, 10% and 1% solutions using DEP. We empirically analysed the results to find relationships of note, by examining RBC response as a function of different medium conductivity, and as a function of chemical modification. Key findings are shown in Fig. 5. When we examined RBCs at common medium ion concentrations, we found strong negative linear correlations between σ_{cyto} and G_{eff}. This was strongest ($r = 0.97$) in lowest conductivity media, with the data for G_{eff} becoming noisier at higher conductivities due to the emergence of an additional low-frequency polarisation in the low-frequency band where G_{eff} dominates (discussed below). This negative correlation tallies with observations reported by Henslee et al.[10], where σ_{cyto} and G_{eff} were observed to vary in antiphase through the day, and suggests that these two parameters have a common origin. We also found a strong dependence between medium conductivity, G_{eff} and C_{eff}. This has been reported in limited fashion for RBCs previously[21] but is not observed in other cells, such as platelets or Jurkats[22]. We found C_{eff} could be modelled empirically to within ± 15% as an additional capacitive layer beyond the membrane with width equal to the double layer thickness. We also observed that G_{eff} varied approximately linearly with ionic strength, indicating a dependence both to this and σ_{cyto}. We found a very significant linear relationship ($r^2 > 0.99$) between V_m and σ_{cyto} for all cases except cells treated with neuraminidase (where $r^2 = 0.86$), of the form $V_m = A - B.\sigma_{cyto}$. We found that A was 85 ± 10% higher in cells without valinomycin than with, whilst B was 47 ± 6% higher in control cells than those in DMSO, suggesting V_m is affected by a change in K^+ transport (in line with Eq. (1)), and DMSO affects how V_m is affected by cytoplasm composition.

Whilst DEP behaviour generally followed the classical models for a shelled spheroid, we observed an increase in polarizability at low frequencies (Fig. 6) similar to that observed in nanoparticles, and attributed to polarisation of the electrical double layer[23]. That paper suggested that the frequency below which the effect occurs depends on a time constant τ. We found that amending the standard model to incorporate this exactly matched our observations. Prior work[23] suggests that τ is inversely proportional to surface conductance k_s. Furthermore, we found a linear relationship (fitted with $r^2 > 0.99$ in all cases) between 1/ τ and ζ', the ζ-potential component due *only* to the surface charge, which followed a linear form of $k_s = P.\zeta' + Q$, with P being 8.9 ± 1.6 × larger in the presence of DMSO than without, and Q being 4.8 ± 1 × larger. This suggests that the low-frequency rise is indeed due to double layer polarisation, and is strongly affected by double layer composition but is unaffected by V_m; it may also suggest that the effect is influenced by both the diffuse layer conduction[24] in term P and Stern layer conduction[23] in term Q.

ζ exhibits an endogenous circadian rhythm. We also examined the variation in ζ over a 48 h period, in comparable conditions to experiments measuring V_m and DEP parameters taken by Henslee et al.[10] Cells in both media demonstrated rhythms (Fig. 6a) when fitted a damped cosinor curve, with periods for of 24 h 53 min (KHB) and 24 h 17 min (DEP medium). The mean values of ζ in were -11.4 mV (KHB)and -24.0 mV (DEP medium). The amplitude of the rhythm in DEP medium was larger at 1.8 mV compared to 0.25 mV in KHB, and the signal was also almost exactly in antiphase (phase difference of 10 h 30 min); this can be explained by

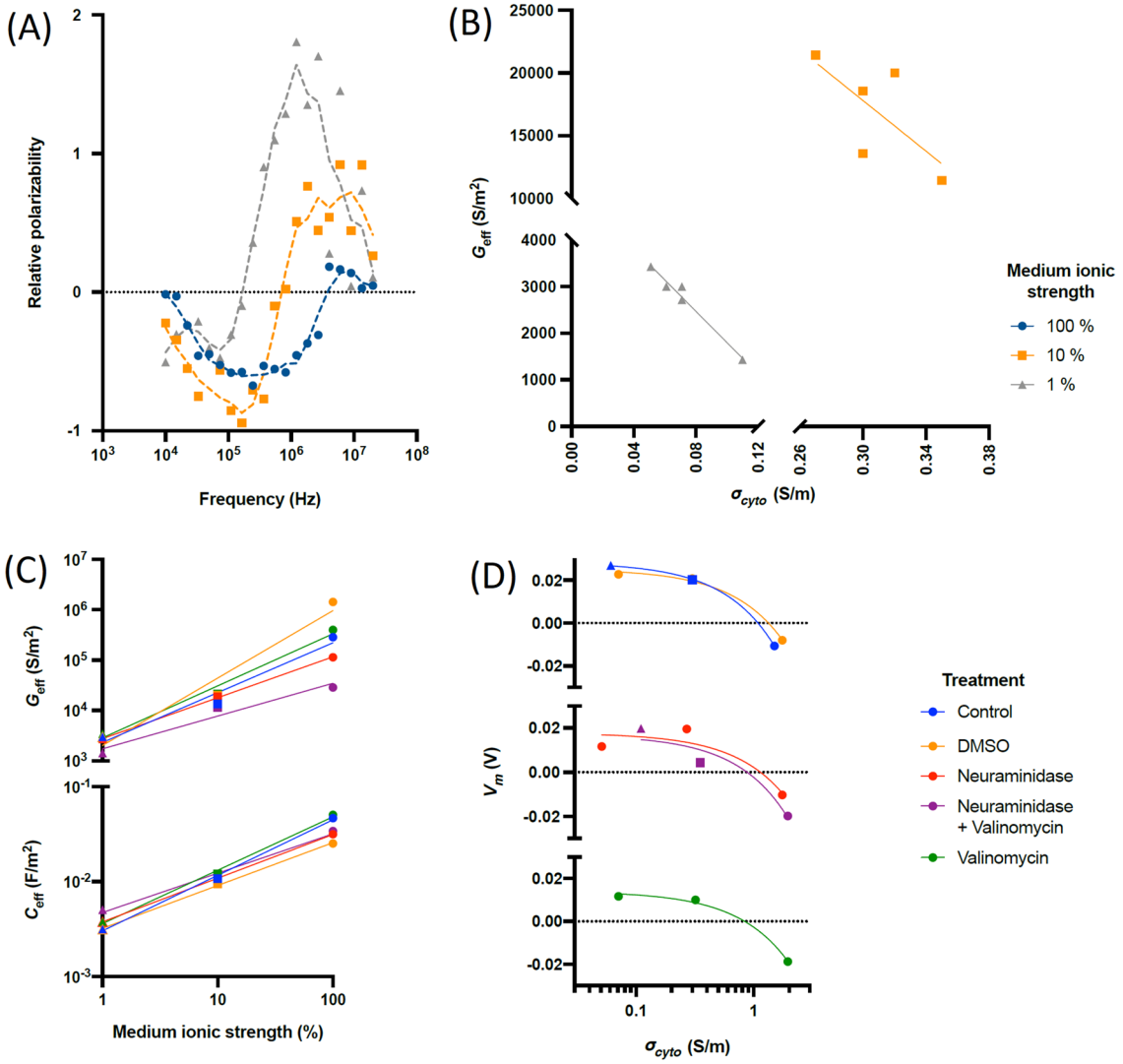

Figure 5. (**A**) The DEP spectra (points) of RBCs in media of different ionic strength (1% (grey), 10% (orange) and 100% (blue)) together with rolling average trendlines; (**B**) the values of G_{eff} vs. σ_{cyto} for 1% and 10% media, together with best-fit trendline; (**C**) Specific membrane conductance G_{eff} and capacitance C_{eff} as a function of medium ionic strength; (**D**) the relationship between cytoplasm conductivity σ_{cyto} and membrane potential V_m.

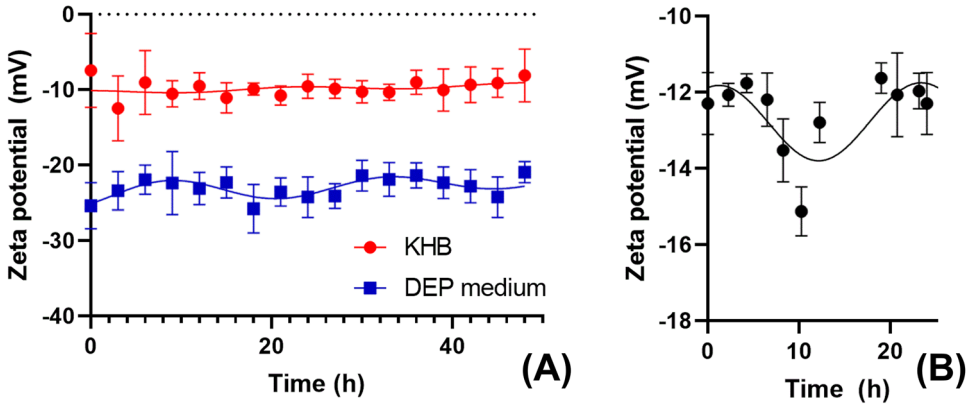

Figure 6. Circadian behaviour of ζ-potential in RBCs. (**A**) mean (n = 4) ζ for RBCs entrained and suspended in KHB and DEP medium, together with best-fit rhythm with period of 24.5 h and 24.3 h respectively. (**B**) ζ of RBCs taken directly from a participant over a 24 h period, measured within 60 s of donation, together with a best-fit rhythm with 22.2 h period (time 0 h corresponds to 10am).

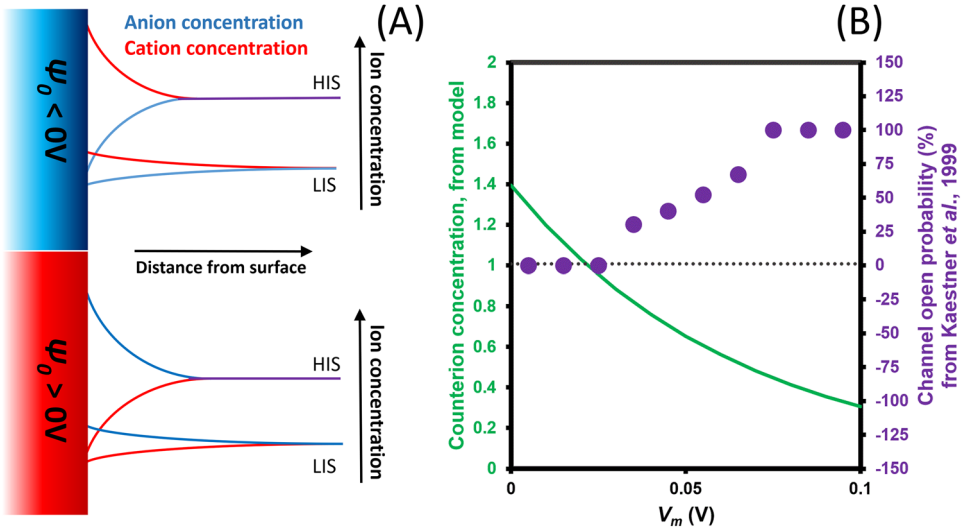

Figure 7. (**A**) A schematic showing ion concentrations in proximity to the cell surface in high ionic strength (HIS) and low ionic strength (LIS) solutions. Where the surface potential of a cell is negative, it will electrostatically attract cations from solution, raising the cation concentration at the surface whilst depleting anions. Where the surface potential is positive, this situation is reversed, with the cation level in HIS solutions reaching similar values to those observed in LIS solutions. (**B**) A comparison of the voltage-gated cation channel behaviour reported by Kaestner et al.[26], and the cation concentration at the surface relative to the bulk (green line) determined using the Poisson-Boltzmann equation, using ζ determined from Eq. (5).

the change in V_m polarity between low- and high-ionic strength media, as described above. The DEP medium rhythm was statistically preferred to a straight line ($p < 0.0001$), though the KHB rhythm was not.

When we examined blood immediately after donation over a 24 h period, we found that ζ again preferentially fitted a damped cosinor ($p > 0.0001$) with a 22 h 9 min period, a -12.9 mV baseline and 1.0 mV amplitude.

If we compare the amplitude of the ζ rhythm in DEP medium with the published data on V_m rhythms by Henslee et al.[10], it suggests a value of Ξ of approximately 0.2; this is lower than calculated for other RBC conditions, though this may be an underestimate due to the relatively low time-precision of the V_m data, or indicative of a reduction in Ξ over the 48 h experimental time after entrainment.

Discussion

The relationship between V_m and ζ can be observed in cells exhibiting voltage-dependent ion channel behaviour without voltage-dependent channels. If there is a causal relationship between V_m and ζ, such that altering V_m alters ζ, which would then have a concomitant effect on V_m, then it raises significant questions about our understanding of V_m and of the validity of the GHK equation. Equation (1) states that V_m is solely dependent on intracellular and extracellular ion concentrations, but not on the current value of V_m; this may need to be adapted to include a feedback component to account for changes in extracellular ion concentration due to V_m.

Evidence for such a relationship may be found in previous electrophysiological studies, where V_m is known and deliberately altered and changes in behaviour observed. For example, the relationship between V_m and ζ provides an explanations for RBC's voltage-dependent, non-specific cation channel, whose function has been observed in patch-clamp experiments[25–27] but whose action has never been correlated with a particular ion transporter. The behaviour of this putative channel is characterised by a cation efflux at holding potentials greater than + 20 mV.

It is also known that RBCs exhibit significant potassium efflux when resuspended in media of low ionic strength[19]. It is important to note that the ion concentration at the cell surface is equal not the concentration in the bulk, as used in the GHK equation, but is instead described by the Poisson-Boltzmann equation (Eq. (4)). This describes diminishing coion concentration and increasing counterion concentration near the surface, as shown schematically in Fig. 7A for positive and negative values of ψ; as can be seen, the high and low ionic strength coion concentrations are similar.

If we replace ψ in Eq. (4) with ζ as determined from Eq. (5) with $\Xi = 0.37$ and $\zeta' = -0.072$ V, we can determine the ion concentration at the shear plane and hence, available for membrane-based ion transporters. Figure 7B shows the cation concentration at the cell surface relative to the bulk. Below $V_m = +19.5$ mV we find cation concentration at the surface is higher than the bulk (whilst anion concentration would be lower); as V_m is elevated beyond this, the cation concentration at the surface drops below that in the bulk, potentially sufficient to shift the cell to elevated ion leakage behaviour as observed in low ionic strength media. Significantly, there is a striking correlation between the surface cation concentration and the "% open probability" for the putative nonspecific

voltage-activated cation channel reported by Kaestner et al.[26] with 100% probability of channel opening coinciding with an external cation concentration of approximately 50% that of bulk medium.

We propose that rather than indicating the presence of a voltage-activated ion channel, the effect is due to V_m altering ζ and hence the ion availability for transport. Furthermore, since changes in the ion permeability due to the low external concentration would cause concomitant elevation in V_m (from the GHK equation), this may make the rise of V_m self-sustaining whilst ion transfer occurs, explaining the hysteresis effect observed in patch-clamp studies of the putative channel[28]. This result is highly significant as it suggests a mechanism describing observed RBC behaviour without requiring any voltage-dependent molecular mechanisms. If the same effect is observed more generally in other cell types, this has significance for our understanding of voltage-activated channels, and also of the GHK equation, dependent as it is on bulk, rather than surface, ion concentrations.

The mechanism of transmission of V_m. The data suggest that electrical properties such as ζ, V_m, G_{eff}, C_{eff} and σ_{cyto} form an interconnected cellular electrome; and that an electric field due to V_m extends beyond the membrane to at least the plane of shear. We can use the data generated from modelling in order to elucidate the physical principles underpinning Ξ.

Classical charged particle theory assumes a solid particle possessing a surface charge. However, a cell is not solid, but rather a membrane with surface charges on both outer and inner faces surrounding a charged core, where the electric field distribution away from the cell is a function of both the surface charge on the outer surface and the surface charge on the inner surface[29]. An obvious potential mechanism for relating V_m to ζ would be if the membrane potential, being dropped across the capacitive membrane, produced charges on the surface in accordance with the principle $Q = CV$; this would then change the surface charge and lead to an altered value of ψ_0 and hence ζ. However this model fails to replicate observed behaviour, since the change in ζ would vary according to the value of $1/\kappa$, and hence with medium ionic strength. This is quite different to our observations, where the additional term ΞV_m appears to be independent of the double layer thickness.

Examination of Ξ shows that values fall broadly into two categories; untreated cells and those treated with neuraminidase have higher values of Ξ (0.19–0.37), whilst cells treated with DMSO or treatments requiring DMSO for resuspension exhibit values of Ξ of approximately 0.08. Cells treated with DMSO also demonstrated lower values of ζ than control, although no mechanism is reported for it altering surface charge. Table 1 also suggests ψ_0 is higher for non-DMSO conditions (control, neuraminidase) than DMSO-treated cells, and differences in behaviour for DMSO-treated vs untreated cells were also observed in the relationship between V_m and σ_{cyto}. DMSO has been reported to cause membrane thinning, and increases membrane fluidity and permeability[30] displacing water at the membrane surface[31], and has a significantly lower relative permittivity than water[32]. Recent examination of the double-layer capacitance surrounding electrodes[33,34] has shown that solution permittivity exhibits a much greater influence on double-layer capacitance than ion concentration, and that the double-layer specific capacitance of DMSO is only 0.14 Fm^{-2} compared with 0.35 Fm^{-2} for water, due to the Stern layer being wider due to the relative size of the solvent molecules (0.37 nm for DMSO, 0.16 nm for water) rather than differences in permittivity ($5.7\varepsilon_0$ for DMSO, $6.3\varepsilon_0$ for water).

We calculated the total capacitance between cell surface and slip plane C_{shear} by assuming a series combination of Stern layer capacitance as described above (assuming that DMSO displaced water at the interface, where used), and a shear plane capacitance calculated using the permittivity of water ($78\varepsilon_0$) and the shear plane thicknesses derived in Table 1. Remarkably, when we compared the inter-condition ratios between the calculated values of capacitance, with the ratios of the estimated values of ψ_{st} we found an exceptionally high degree of correlation (Table 1). We suggest that this strongly validates both the model of capacitance between membrane and shear plane.

Furthermore, when we developed empirical models to elucidate physical principles underlining Ξ, we found we were able to obtain excellent fits using the equation:

$$\Xi = \frac{\alpha C_{shear}^2}{1 + C_{shear}^2} \tag{6}$$

where α is a dimensionless constant of value 6.7. This produced values of Ξ of 0.34 for control cells, 0.19 for neuraminidase-treated cells, and 0.065–0.10 for the three DMSO treatment conditions. Interestingly, The dependence on the *square* of the capacitance is echoed in the relationship between potential and capacitance in semiconductor physics of PN junctions, in which a potential is applied across a barrier comprising different concentrations of positive and negative charge carriers, suggesting that this may be a route to a more analytical model of Ξ.

The physiological implications of ζ dependence on V_m. The modification of ζ by V_m may explain phenomena such as the "storage lesion" in blood-banked RBCs, where storage results in cells reducing in ζ-potential without a commensurate loss of sialic acid from the membrane[17,35], may be due to loss of cytosolic K^+ in the days following storage[36], causing a depolarization of V_m leading to a reduction loss in ζ. ζ has also been implicated in the formation of rouleaux[15,16]; our results suggest that changing either the permittivity of the double layer or the value of V_m may modulate this behaviour. This is consistent with observations that the erythrocyte sedimentation rate (ESR) of whole blood is modulated by K^+ channel blockers such as quinine[37].

Whilst we observed changes in ζ in both entrained and ex vivo samples, there are no reports in the literature of circadian behaviour in blood sample measurements of ζ, or of the most common clinical measurement in which ζ takes a role, that of erythrocyte sedimentation rate. One possible reason for this is that changes in ζ are a mechanism for pre-emptive adaptation to changing conditions in plasma in normal physiology. This would allow RBCs to compensate for circadian changes in blood plasma composition, maintaining a constant level of

Solution	NaCl		KCl		NaCl + KCl			$CaCl_2$	
Ion	Na	Cl	K	Cl	Na	K	Cl	Ca	Cl_2
[mM]o	145	145	145	145	72.5	72.5	145	0.97	0.97
[mM]i	11	80	140	80	11	140	80	0.0057	80
pX	54	21	100	21	54	100	21	50	21

Table 3. Table of ion concentrations used in calculations. The ion concentrations used in GHK modelling to determine the membrane potential in different ionic solutions.

electrostatic repulsion throughout the day. However, since this relies on two unconnected systems maintaining common rhythms, desynchronization in either amplitude or phase could potentially present dangers. It is notable that the period of the observed cycle where ζ is least polarised is between 0700 – 1200, the time window most associated with cardiovascular disease events such as heart attacks and strokes[38]. Further investigation on this topic, particularly considering in vivo measurements, may yield clinically beneficial information.

More speculatively, if the relationship between V_m and ζ occurs across other cell types, it may explain observed behaviours where cells exhibit changes in V_m when altering the way in which they interact with their environment. There is evidence to suggest this; it was recently shown that HeLa cells change ζ when subject to heat shock[36], which our results suggest correlates to depolarisation due to loss of membrane integrity. Furthermore, several cell types exhibit changes in V_m when altering the way in which they interact with their environment. For example, as cancer cells increase in metastatic potential, their membrane potentials become more depolarised[6], whilst membrane capacitance increases[8]; changes in V_m have been reported upon activation in macrophages[39] and platelets[40]; ova of many species also change V_m immediately after fertilization[41]. Human sperm infertility has been associated both with low ζ[42] and low membrane potential[43], which our model suggests may be different measures of the same phenomenon. All of these cases correspond to cells which seek either to move into contact with other cells (platelets, macrophages) or else repel other cells (metastasising cancer cells, fertilised eggs), a process in which ζ may play a significant role.

In summary, we demonstrate an endogenously-generated electric field proportional to the membrane potential, and most likely caused by capacitive coupling between cytoplasm and extracellular medium, which manifests as changes in ζ-potential, low-frequency polarisation and surface conductance. Significantly, this shows RBCs can alter the way in which they interact with their surroundings by V_m rather than membrane composition, shedding new light on ion channel activity, cardiovascular disease, and drug action.

Methods

Goldman–Hodgkin–Katz (GHK) modelling. V_m was calculated using an adapted GHK equation. Extracellular ion concentrations were as below in 'media'. Where an ion was absent from an extracellular solution, the concentration was set as 0 mM. Internal ion concentrations (mM) for RBCs[44] were taken as: 140 K^+, 11 Na^+, 80 Cl^-, and 0.006Ca^{2+}. Relative permeabilities[45] were taken as 100 for K^+, 54 for Na^+, 21 for Cl^- and 50 for Ca^{2+}. Further details can be found in Table 3.

Blood cell preparation. Studies were conducted in accordance with the principles of the Declaration of Helsinki, with a favourable ethical opinion from the Research Ethics Committee at the University of Surrey. Participants in the study were screened for relevant self-reported health issues, including sleep disorders or excessive daytime sleepiness. Participants provided written, informed consent after having received a detailed explanation of the study procedures. RBCs were isolated from anticoagulant-treated whole blood by density gradient centrifugation layering a mixture of whole blood and PBS (1:3) on top of Histopaque-1077 (1.077 g/ml polysucrose solution) (Sigma-Aldrich, St Louis, MO) according to manufacturer's instructions. RBCs were washed twice in PBS before resuspension in Krebs–Henseleit buffer (KHB, pH 7.4, 290 mOsm) (Sigma-Aldrich). These minimal medium conditions ensure the tiny fraction of nucleated cells detectable in RBC pellets immediately after centrifugation (~ 0.02%) undergo cell death in < 24 h and cannot influence RBC circadian rhythms, which is comparable to granulocyte depletion using anti-CD15 beads confirmed by gel zymography[10]. Circadian entrainment was achieved by 12:12 h 32 °C:37 °C temperature cycles over 48 h using a thermal cycler, and then used for experiments.

Media and drug treatments. Isosmotic media were prepared for three experiments. In the first experiment, a physiological-strength ionic solution was prepared containing 145 mM NaCl and 7.5 mM KCl; this is referred to as the "100% solution" in the text. A second medium was prepared by diluting this 1:9 (final concentration 14.5 mM NaCl and 0.75 mM KCl) and a third, 1:99 using an isomotic solution containing 8.5% w/v sucrose and 0.5% w/v dextrose. These are referred to as the 10% and 1% solutions, respectively. For the second experiment, solutions were prepared of 145 mM KCl, 145 mM NaCl, 97 mM $CaCl_2$ or a mixture containing 72.5 mM KCl and 72.5 mM NaCl. Cells were left to equilibrate with the media for 30 min prior to measurement, except where described in the text. For the third experiment, RBCs were suspended either in KHB as described above, or a low-conductivity "DEP medium" comprising an iso-osmotic sucrose-glucose solution adjusted to a conductivity of 0.043 S/m[10] using phosphate-buffered saline (Labtech International, Heathfield, UK). In addition to untreated control cells, four treatments were used: neuraminidase (15ug/ml final concentration); valinomycin

(30 nM final concentration) dissolved in DMSO; a combined treatment of both valinomycin and neuraminidase together; and a DMSO vehicle control (0.13%). All treatments were incubated for 30 min before measurement.

Circadian rhythm analysis. RBCs were incubated at constant 37 °C for time course sampling, with a separate aliquot being removed from the cycler for analysis at each time point for each donor. The final transition to 37 °C was taken as t = 0 (or Zeitgeber time 0, ZT0). Measurements were taken every 3 h from ZT0 to ZT48. We also tested a single participant using blood taken via needlestick to the finger, approximately every 2 h for 24 h; a drop of blood was resuspended in 1 ml KHB and measured the ζ-potential immediately, with 3 measurements taken as before. Time course data were analysed using Prism 8 (Graphpad Software, La Jolla, CA). Curve fitting was used to fit a damped cosine in order to determine the circadian parameters baseline, period, amplitude and phase as described by Hirota et al.[46]; to determine if a circadian rhythm was present, a straight line fit (y = mx + c) was compared with a damped cosine + baseline fit (y = mx + c + amplitude x e(-kx) x cos(2.π.(X-phase)/period)) using the extra sum-of-squares F test in the compare models function of Prism 8, with the simpler model being preferred unless the p value was < 0.05.

Measurement protocols. Data collection was performed using three methods in parallel, timed to ensure that measurements were as close in time to one another as possible (within 1 min).

Passive electrical properties. Passive electrical properties were measured using dielectrophoresis (DEP)[47]. The cell population was counted using a haemocytometer and adjusted to 1.15×10^6 cells/ml (± 15%). 100 cell radii were measured using Image J software (National Institute of Health, Maryland, US) for use in the analysis. Cell suspensions were analysed using a 3DEP reader (Heathfield, UK)[22]. Cells were analysed for 60 s at five points per decade (10 kHz—20 MHz). Five technical repeats were performed for each of the four donors taken, and all data were averaged before fitting to a single-shell model[48] using MATLAB (The Mathworks, USA) to determine C_{eff}, G_{eff} and σ_{cyto}. The model was adapted[23,24] to include the contribution from the low-frequency double layer polarization observed in nanoparticles.

ζ-Potential. Z was measured using the dynamic light scattering method[49]. Samples were pipetted into disposable cuvettes and analysed using a Malvern Panalytical Zetasizer Nano ZS90 (Malvern, UK). Six technical repeats were taken per sample.

Membrane potential. V_m was determined using the CCCP (carbonylcyanide-m-chlorophenylhydrazone) method (Moersdorf et al.[19]), which allows rapid determination in a variety of media, including low ionic strengths where patch-clamp would be unable to form a suitable seal. To measure V_m, 200 µl of packed cells were added to 4.8 mL of the test solution together with 20 µM (final concentration) of CCCP in a DMSO carrier. V_m was determined by monitoring of extracellular pH (pH_{out}) in the presence of CCCP using a conventional pH electrode and calculated using the equation: $V_m = 61.5\ mV \times (pH_{in} - pH_{out})$. Due to the high RBC buffer capacity, the intracellular pH (pH_{in}) remains constant throughout the experiment. Final pH was determined as the pH in the solution after the cells were lysed by addition of 200 µl Triton X-100 (1% v/v) in 2 M NaCl solution.

Received: 26 May 2021; Accepted: 25 August 2021
Published online: 30 September 2021

References

1. Galvani, L. *De viribus electricitatis in motu musculari commentarius* (Ex Typographia Instituti Scientiarum; 1792).
2. Nernst, W.H. *Die elektromotorische wirksamkeit der Jonen* (W. Engelmann, 1889).
3. Goldman, D. E. Potential, impedance, and rectification in membranes. *J. Gen. Physiol.* **27**, 37–60 (1943).
4. Hodgkin, A. L. & Katz, B. The effect of sodium ions on the electrical activity of the giant axon of the squid. *J. Physiol.* **108**, 37–77 (1949).
5. Hodgkin, A. L. & Huxley, A. F. A quantitative description of membrane current and its application to conduction and excitation in nerve. *J. Physiol.* **117**, 500–544 (1952).
6. Yang, M. & Brackenbury, W. J. Membrane potential and cancer progression. *Front. Physiol.* **4**, 185. https://doi.org/10.3389/fphys.2013.00185 (2013).
7. Hodgkin, A. L. & Huxley, A. F. Action potentials recorded from inside a nerve fibre. *Nature* **144**, 710–711 (1939).
8. Liang, X., Graham, K. A., Johannessen, A. C., Costea, D. E. & Labeed, F. H. Human oral cancer cells with increasing tumorigenic abilities exhibit higher effective membrane capacitance. *Integr. Biol.* **6**, 545–554 (2014).
9. Labeed, F. H. *et al.* Biophysical characteristics reveal neural stem cell differentiation potential. *PLoS ONE* **6**, e25458. https://doi.org/10.1371/journal.pone.0025458 (2011).
10. Henslee, E. A. *et al.* Rhythmic potassium transport regulates the circadian clock in human red blood cells. *Nat. Commun.* **8**, 1978. https://doi.org/10.1038/s41467-017-02161-4 (2017).
11. Beale, A. D. *et al.* Casein Kinase 1 underlies temperature compensation of circadian rhythms in human red blood cells. *J. Biol. Rhythm.* **34**, 144–153 (2019).
12. Lyklema, J. *Fundamentals of Interface and Colloid Science* (Academic Press, 1991).
13. Stern, O. Zur Theorie der Elektrolytischen Doppelschicht. *Z. Elektrochemie* **30**, 504–508 (1924).
14. Booth, F. Theory of electokinetic effects. *Nature* **161**, 83–86 (1948).
15. Izumida, Y., Seiyama, A. & Maeda, N. Erythrocyte aggregation: Bridging by macromolecules and electrostatic repulsion by sialic acid. *Biochim. Biophys. Acta* **1067**, 221–229 (1991).
16. Bäumler, H., Neu, B., Donath, E. & Kiesewetter, H. Basic phenomena of red blood cell rouleaux formation. *Biorheology* **36**, 439–442 (1999).
17. Huang, Y.-X. *et al.* Human red blood cell aging: Correlative changes in surface charge and cell properties. *J. Cell Mol. Med.* **15**, 2634–2642 (2011).

18. Bernhardt, I. & Ellory, C. J. *Red Cell Membrane Transport in Health and Disease* (Springer-Verlag, 2003).
19. Moersdorf, D. *et al.* Transmembrane potential of red blood cells under low ionic strength conditions. *Cell Physiol. Biochem.* **31**, 875–882 (2013).
20. Jan, K.-M. & Chien, S. Role of surface electric charge in red blood cell interactions. *J. Gen. Physiol.* **61**, 638–654 (1973).
21. Gascoyne, P., Pethig, R., Satayavivad, J., Becker, F. F. & Ruchirawat, M. Dielectrophoretic detection of changes in erythrocyte membranes following malarial infection. *Biochim. Biophys. Acta.* **1323**, 240–252 (1997).
22. Hoettges, K. F. *et al.* Ten–second electrophysiology: Evaluation of the 3DEP Platform for high-speed, high-accuracy cell analysis. *Sci. Rep.* **9**, 19153. https://doi.org/10.1038/s41598-019-55579-9 (2019).
23. Hughes, M. P. Dielectrophoretic behaviour of latex nanospheres: Low-frequency dispersion. *J. Coll. Int. Sci.* **250**, 291–294 (2002).
24. Hughes, M. P., Morgan, H. & Flynn, M. F. The dielectrophoretic behavior of submicron latex spheres: Influence of surface conductance. *J. Coll. Int. Sci.* **220**, 454–457 (1999).
25. Christophersen, P. & Bennekou, P. Evidence for a voltage-gated, non-selective cation channel in the human red cell membrane. *Biochim. Biophys. Acta.* **1065**, 103–106 (1991).
26. Kaestner, L., Bollensdorff, C. & Bernhardt, I. Non-selective voltage-activated cation channel in the human red blood cell membrane. *Biochim. Biophys. Acta.* **1417**, 9–15 (1999).
27. Rodighiero, S., De Simoni, A. & Formenti, A. The voltage-dependent nonselective cation current in human red blood cells studied by means of whole-cell and nystatin-perforated patch-clamp techniques. *Biochim. Biophys. Acta.* **1660**, 164–170 (2004).
28. Richter, S., Hamann, J., Kummerow, D. & Bernhardt, I. The Monovalent cation "Leak" transport in human erythrocytes: An electroneutral exchange process. *Biophys. J.* **73**, 733–745 (1997).
29. Dharmasena, R. D. I. G. *et al.* Triboelectric nanogenerators: Providing a fundamental framework. *Energy Environ. Sci.* **10**, 1801–1811 (2017).
30. Yu, Z.-W. & Quinn, P. J. Solvation effects of dimethyl sulfoxide on the structure of lipid bilayers. *Biophys. Chem.* **70**, 35–39 (1998).
31. Cheng, C.-Y., Song, J., Pas, J., Meijer, L. H. H. & Han, S. DMSO induces dehydration near lipid membrane surfaces. *Biophys. J.* **109**, 330–339 (2015).
32. Lide, D. R. (ed.) *Handbook of Chemistry and Physics* 83rd edn. (CRC Press, 2002).
33. Hou, Y., Aoki, K. J., Chen, J. & Nishiumi, T. Solvent variables controlling electric double layer capacitance at the metal-solution interface. *J. Phys. Chem. C.* **118**, 10153–10158 (2014).
34. Hou, Y. *Controlling Variables of Electric Double-Layer Capacitance* (University of Fukui, 2014).
35. Silva, D. C. N. *et al.* Optical tweezers as a new biomedical tool to measure zeta potential of stored red blood cells. *PLoS ONE* **7**, e31778. https://doi.org/10.1371/journal.pone.0031778 (2012).
36. Antwi-Baffour, S. *et al.* A study of the change in sodium and potassium ion concentrations in stored donor blood and their effect on electrolyte balance of recipients. *BioMed Res. Int.* https://doi.org/10.1155/2019/8162975 (2019).
37. Robbins, R. C. & Harbin, J. E. Jr. The in vitro sensitivity of erythrocyte aggregation to quinine: Assessment by a serial blood sedimentation procedure. *Clin. Chem.* **17**, 31–33 (1971).
38. Elliot, W. J. Cyclic and circadian variations in cardiovascular events. *Am. J. Hypertens.* **14**, 291S-295S (2001).
39. Li, C., Levin, M. & Kaplan, D. L. Bioelectric modulation of macrophage polarization. *Sci. Rep.* **6**, 21044. https://doi.org/10.1038/srep21044 (2016).
40. Pales, J., Lopez, A. & Gual, A. Platelet membrane potential as a modulator of aggregating mechanisms. *Biochim. Biophys. Acta* **944**, 85–89 (1988).
41. Iwao, Y. & Jaffe, L. A. Evidence that the voltage-dependent component in the fertilization process is contributed by the sperm. *Dev. Biol.* **134**, 446–451 (1989).
42. Esfahani, M. H. N., Deemeh, M. R., Tavalee, M., Sekhavati, M. H. & Gourabi, H. Zeta sperm selection improves pregnancy rate and alters sex ratio in male factor infertility patients: A double-blind, randomized clinical trial. *Int. J. Fertil. Steril.* **10**, 253–260 (2016).
43. Brown, S. G. *et al.* Depolarization of sperm membrane potential in a common feature of men with subfertility and is associated with low fertilization rate at IVF. *Hum. Reprod.* **31**, 1147–1157 (2016).
44. Hoffman, J. F. Active transport of Na^+ and K^+ by red blood cells. In *Physiology of Membrane Disorders* 2nd edn (eds Andreoli, T. E. *et al.*) (Springer, 1986).
45. London, R. D., Lipkowitz, M. S., Sinert, R. H. & Abramson, R. G. Modulation of ionic permeability in a nonpolarized cell: Effect of cAMP. *Am. J. Physiol.* **257**, F985-993 (1989).
46. Hirota, T. *et al.* A chemical biology approach reveals period shortening of the mammalian circadian clock by specific inhibition of GSK-3beta. *Proc. Natl. Acad. Sci. USA* **105**, 20746–20751 (2008).
47. Pethig, R. *Dielectrophoresis: Theory, Methodology and Biological Applications* (Wiley, 2017).
48. Broche, L., Labeed, F. H. & Hughes, M. P. Extraction of dielectric properties for multiple populations from dielectrophoretic collection spectrum data. *Phys. Med. Biol.* **50**, 2267–2274 (2005).
49. Gittings, M. R. & Saville, D. A. The determination of hydrodynamic size and zeta potential from electrophoretic mobility and light scattering measurements. *Coll. Surf A.* **141**, 111–117 (1998).

Acknowledgements

We thank Dr Lisa Flanagan (University of California Irvine) and Professor Ronald Pethig (University of Edinburgh) for valuable discussions.

Author contributions

M.P.H. originated and developed the model, analysed data, took ζ measurements, and wrote the paper. Z.P.T. collected ζ measurements and modelled DLVO and long-range effects. S.Q. and P.A. took ζ data. E.J.K. collected and modelled DEP and CCCP data. E.A.H. identified the DEP effect in preliminary measurements. S.J.K. took DEP data. A.D.B. took CCCP data and co-ordinated experiments. R.A.D. co-developed the theory. O.C. performed data analysis. R.L. performed the GHK calculations. F.H.L. took CCCP and DEP data and organised the experiments.

Competing interests

MPH is a director of Deparator, which manufactures the 3DEP instrument used for the DEP measurements. The authors declare no other interests.

Additional information

Correspondence and requests for materials should be addressed to M.P.H.